Wave Motion 106 (2021) 102779

Contents lists available at ScienceDirect

Wave Motion

journal homepage: www.elsevier.com/locate/wamot

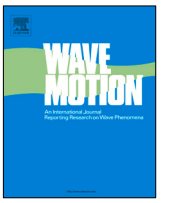

Breather arrest in a chain of damped oscillators with Hertzian contact

Matteo Strozzi [a,b], Oleg V. Gendelman [b,*]

[a] Department of Sciences and Methods for Engineering, University of Modena and Reggio Emilia, Italy
[b] Faculty of Mechanical Engineering, Technion - Israel Institute of Technology, Technion City, Haifa 3200003, Israel

ARTICLE INFO

Article history:
Received 23 June 2020
Received in revised form 22 April 2021
Accepted 1 June 2021
Available online xxxx

Keywords:
Breather arrest
Oscillatory chain
Hertzian contact
Viscous damping
Nonlinear beatings

ABSTRACT

Breather propagation in a damped oscillatory chain with Hertzian nearest-neighbour coupling is investigated. The breather propagation exhibits an unusual two-stage pattern. The first stage is characterized by power-law decay of the breather amplitude. This stage extends over finite number of the chain sites. Drastic drop of the breather amplitude towards the end of this finite fragment is referred to as *breather arrest*. At the second stage, the breather exhibits very small amplitudes with hyper-exponential decay. Numeric results are rationalized by considering a simplified model of two damped linear oscillators coupled by Hertzian contact forces. Initial excitation of one of these oscillators results in a finite number of beating cycles in the system. This simplified model reliably predicts main features of the breather arrest. More general coupling potentials and effect of pre-compression on the breather propagation are also discussed.

1. Introduction

Spatially localized excitations propagating in nonlinear lattices, such as solitary waves and breathers, have attracted a lot of interest in recent years, from purely theoretical viewpoint, as well as in view of versatile applications including electro-mechanical devices, e.g. shock and energy absorbers [1–4], actuators and sensors [5,6], acoustic lenses and diodes [7,8].

Strictly speaking, the breathers are most commonly defined as spatially localized time-periodic oscillations arising in nonlinear lattices due to the simultaneous presence of spatial discreteness, nonlinearity and local potentials [9–19]. In this paper, however, we follow some previous studies and somewhat freely use the term "breather" for substantially localized oscillatory wave package travelling through the nonlinear chain. This term usage is more or less traditional [20,21]. Several analytical and numerical studies address the travelling breathers in different types of nonlinear lattices, e.g. Klein–Gordon lattices [22–24], Fermi–Pasta–Ulam lattices [25–27] and granular lattices [28–30].

Primarily, the breathers are considered in conservative lattices. However, in practical applications, the dissipation cannot be neglected and therefore external/internal excitations should counter-balance the energy dissipation to preserve the breather solution [9,10]. Most non-conservative, multi-degree-of-freedom (multi-DOF) nonlinear systems possessing the discrete breathers usually can be analysed only by means of numerical computations or approximate analytical methods [9,16]. Conversely, there are very few damped-forced dissipative models of vibro-impact lattices where some exact analytical solutions for the discrete breathers were derived [14,17–19].

* Corresponding author.
E-mail address: ovgend@technion.ac.il (O.V. Gendelman).

https://doi.org/10.1016/j.wavemoti.2021.102779
0165-2125/

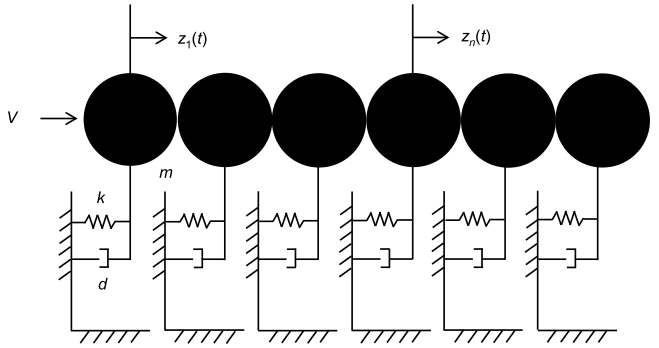

Fig. 1. Sketch of the granular chain with on-site elastic stiffness and damping (no pre-compression).

The presence of damping without external excitations inevitably leads to the energy dissipation and therefore decay of the breather. In the case of linear viscous damping, one intuitively expects that this amplitude decay will be exponential. However, recently it was demonstrated [31] that if the coupling between the nearest neighbours is essentially nonlinear (i.e. non-linearizable), then, due to peculiar interaction between these two factors (essential nonlinearity and damping) one observes an interesting phenomenon of *breather arrest* (BA). Based on the findings presented below, the BA can be defined as abrupt crossover from power-law to hyper-exponential decay of the maximum breather amplitude, leading to a negligibly small amplitude after penetration of the breather to *finite* depth in the lattice [31]. This result has been obtained for somewhat exotic (albeit physically realizable) case of purely cubic coupling.

Main goal of current study is the generalization of these results, and, in particular, the exploration of the BA phenomenon in a chain with Hertzian contact coupling and linear damped elastic foundation. Hertzian contact forces attract a lot of attention, since they are ubiquitous and easily realizable in experiments, and in the same time exhibit a plethora of important nonlinear phenomena, including the breather propagation [1–5,28–30,32–34]. In particular, it was demonstrated that the breathers in nonlinear lattices with Hertzian contact between the oscillators in the absence of pre-compression reveal themselves due to existence of parabolic on-site potentials [35]. These theoretical models are directly related to recent experiments on the pulse propagation in Hertzian chains mounted on elastic flexures [36] or embedded into a viscoelastic medium [37,38].

The structure of the paper is as follows. In Section 2, the BA phenomenon in a chain of linear damped oscillators with Hertzian contact coupling is demonstrated and explored numerically; main scaling relationships are revealed. In Section 3, the BA phenomenon is related to the dynamics of beatings in a pair of linear damped oscillators with Hertzian coupling. This last system is simple enough to allow direct analytic exploration and offers quantitative explanations to the observed regularities of the breather propagation. Section 3 is followed by Conclusions.

2. Description of the model and numeric results

Let us consider a chain of N identical oscillators with mass m grounded by means of linear springs and viscous dampers with elastic stiffness and damping coefficient k and d, respectively; $z_n(t)$ is the displacement of the nth oscillator. Adjacent oscillators in dynamics equilibrium are in contact with possible initial overlap $r \geq 0$ (pre-compression). If the pre-compression is not zero, it is assumed that constant forces are applied to the terminal particles to maintain the homogeneous state of equilibrium. The contact interaction between them is assumed to be Hertzian, which is described by the following force function:

$$F_{n,n+1} = \begin{cases} C \cdot q_{n,n+1}^{3/2}, & q_{n,n+1} > 0 \\ 0, & q_{n,n+1} \leq 0, \end{cases} \qquad q_{n,n+1} = r + z_n(t) - z_{n+1}(t) \tag{1}$$

The system is excited by instantaneous impact to the leftmost oscillator, after which it obtains initial velocity V, as shown in Fig. 1.

The system is non-dimensionalized in the following way:

$$t = \omega_n^{-1}\tau, \quad z_n = \alpha u_n, \quad r = \alpha\delta, \quad k = m\omega_n^2, \quad \lambda = \frac{d}{m\omega_n}, \quad \alpha = \left(\frac{k}{C}\right)^2 > 0 \tag{2}$$

where $(\tau,\ u_n,\ \delta)$ represent the non-dimensional time, displacement of the nth oscillator and initial pre-compression, respectively, ω_n is the natural frequency of the oscillators, α denotes the displacement scale and λ is the non-dimensional damping coefficient.

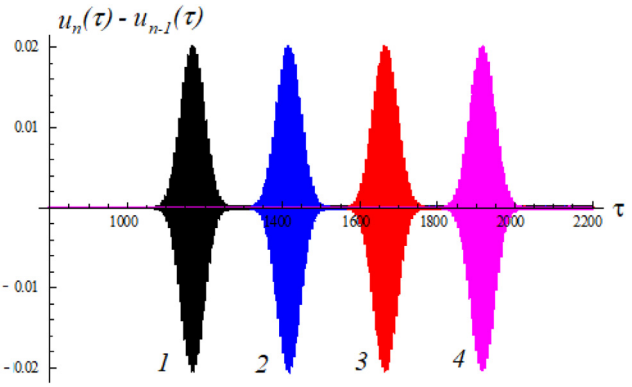

Fig. 2. Propagation of the undamped breather in the chain of oscillators with Hertzian contacts. Initial amplitude A = 0.03, the displacement difference between the particles is plotted for n = 50 (1, black), n = 60 (2, blue), n = 70 (3, red) and n = 80 (4, purple). (For interpretation of the references to colour in this figure legend, the reader is referred to the web version of this article.)

Equations of motion of the system in non-dimensional form are written as follows:

$$\begin{cases} \ddot{u}_1 + u_1 + \lambda\dot{u}_1 + f\,(\delta + u_1 - u_2) = f\,(\delta) \\ \ddot{u}_n + u_n + \lambda\dot{u}_n + f\,(\delta + u_n - u_{n+1}) - f\,(\delta + u_{n-1} - u_n) = 0,\ \ 2 \le n \le N-1 \\ \ddot{u}_N + u_N + \lambda\dot{u}_N - f\,(\delta + u_{N-1} - u_N) = -f\,(\delta) \end{cases}$$
$$f\,(x) = \begin{cases} x^{3/2}, & x > 0 \\ 0, & x \le 0 \end{cases} \tag{3}$$

where the dot symbol denotes differentiation with respect to τ.

Non-dimensional initial conditions for system (3) are written as:

$$\begin{cases} u_n(0) = 0,\ \ 1 \le n \le N \\ \dot{u}_n(0) = 0,\ \ 2 \le n \le N \\ \dot{u}_1\,(0) = A \end{cases} \tag{4}$$

with $A = V/(\alpha\omega_n)$.

The presence of on-site elastic potentials within the oscillatory chain of Fig. 1, together with the Hertzian interactions between the nearest neighbour oscillators, implies the existence of breathers [35]. At the first stage, we simulate the dynamics of system (3) under initial conditions (4) with the help of *Wolfram Mathematica 9* [39] using the Runge–Kutta iterative method.

First, let us assume zero pre-compression and zero damping ($\delta = 0, \lambda = 0$). For relatively low initial excitation, one obtains the propagation of an undamped breather, as presented in Fig. 2.

The initial excitation level is rather low, compared to the simulations with nonzero damping presented below. One observes that the breather travels through the lattice without substantial decay. Similar results for the breather propagation in conservative chain were reported in recent paper [40] for the case of linear oscillators with cubic coupling.

Fig. 3 presents a typical response for the chain element if the damping is present. The amplitude of displacement is very close to zero in the initial time region, then it attains maximum value $A_{\max}$ and finally decreases. Note that in this case the breather propagation is strongly hindered — even at cite n = 6 the maximum breather amplitude is by order of magnitude lower than the initial excitation value.

Fig. 4 describes the decay of maximum amplitude $A_{\max}$ of the travelling breather while propagating along the chain. One clearly observes the sharp transition from steady decay to almost zero amplitude at certain penetration depth. This simulation illustrates the phenomenon of the breather arrest.

As for any crossover effect, it is hardly possible to define exactly the precise value of the arrest site. For the purposes of initial estimation and illustration, and somewhat arbitrary, we identify the BA when the maximum amplitude $A_{\max}$ assumes a value lower than the breather arrest threshold, which is chosen as $A_{\text{arrest}} = A/1000$. In Section 3 we argue that the breathers are initialized only for not too large values of the initial excitation, namely A should not exceed unity; this conclusion nicely conforms to the numeric results. With this restriction in mind, additional simulations demonstrate that the results are barely modified if the threshold is changed by order of magnitude in either direction. In what follows, we discuss a more refined procedure for the numeric identification of the BA, based on an asymptotic approximation for the decay of the breather amplitude. In the case reported in Fig. 3, the BA is obtained at the penetration depth $n_{\text{arrest}} = 9$ where $A_{\max} \approx 5\times10^{-4}$.

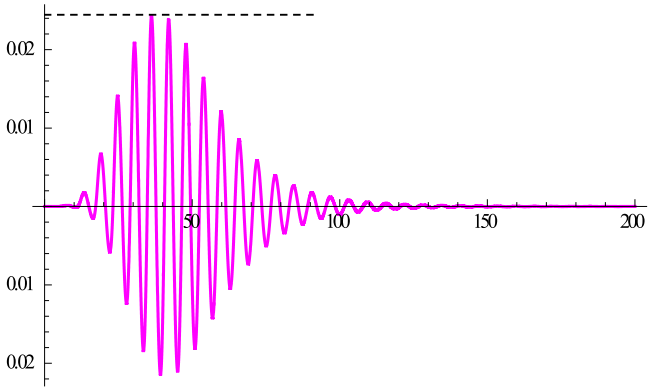

Fig. 3. Time series for the oscillator $n = 6$. $A = 0.5$, $\lambda = 0.1$, $N = 20$. Maximum amplitude $A_{\max} = 0.02428$.

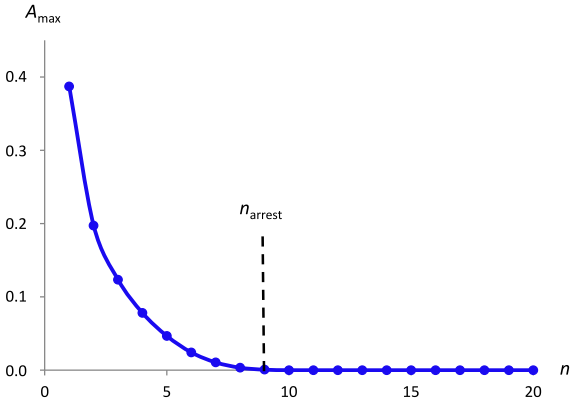

Fig. 4. Breather maximum amplitude $A_{\max}$ vs. corresponding nth oscillator. $A = 0.5$, $\lambda = 0.1$. BA threshold $A_{\text{arrest}} = 5\times10^{-4}$. BA depth $n_{\text{arrest}} = 9$.

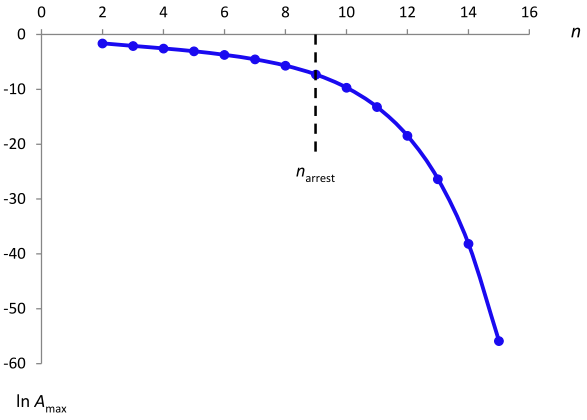

Fig. 5. Breather maximum amplitude $A_{\max}$ vs. n in semi-logarithmic coordinates. $A = 0.5$, $\lambda = 0.1$. BA threshold $A_{\text{arrest}} = 5\times10^{-4}$. BA depth $n_{\text{arrest}} = 9$.

In order to elucidate the asymptotic nature of the BA phenomenon, data from Fig. 3 are re-plotted in semi-logarithmic scale ($\ln A_{\max}$ vs. n) in Fig. 5 , and in double-logarithmic scale for modified coordinates ($\ln A_{\max}(n)$ vs. $\ln (n_{\text{arrest}} - n)$ for $n < n_{\text{arrest}}$) in Fig. 6.

In Fig. 5, one clearly observes a very rapid, hyper-exponential decay of the breather amplitude for $n > n_{\text{arrest}}$. Therefore, one can conclude that the breather propagation along the chain is clearly divided into two stages with a qualitatively different asymptotic behaviour — from the power-law to the hyper-exponential decay. However, in Fig. 5 no apparent

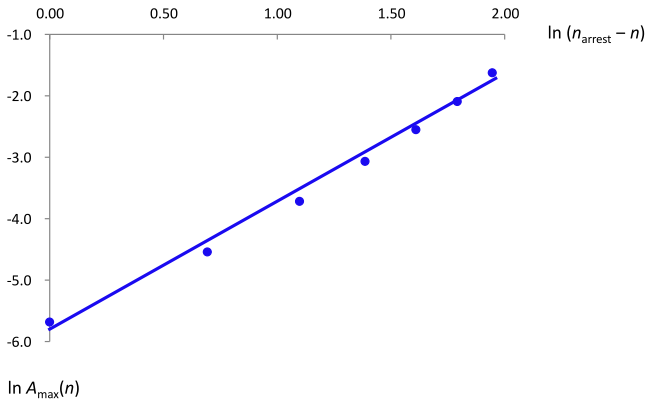

Fig. 6. Breather maximum amplitude $A_{\max}(n)$ vs. $(n_{\text{arrest}} - n)$ in logarithmic coordinates. $A = 0.5$, $\lambda = 0.1$. BA threshold $A_{\text{arrest}} = 5\times10^{-4}$. BA depth $n_{\text{arrest}} = 9$.

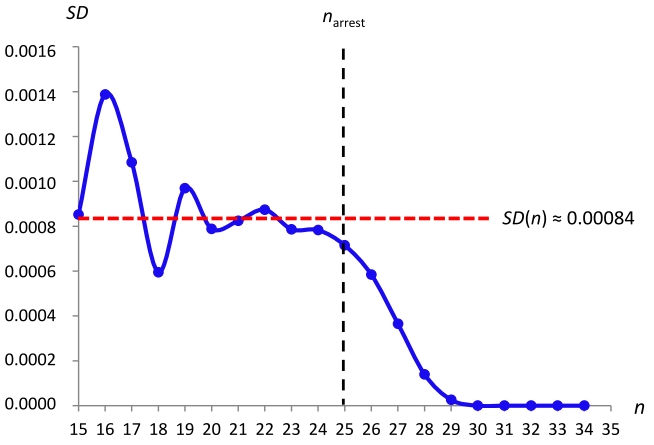

Fig. 7. The second difference (6) of the breather maximum amplitudes. $A = 0.7$, $\lambda = 0.03$. BA threshold $A_{\text{arrest}} = 7\times10^{-4}$. BA depth $n_{\text{arrest}} = 25$.

fitting is noted. As for the fragment $n < n_{\text{arrest}}$, according to Fig. 6, one can adopt a linear fitting between $\ln A_{\max}(n)$ and $\ln (n_{\text{arrest}} - n)$, with the approximate slope $m = 2.08$.

Thus, one can conjecture that the decay of the breather maximum amplitude at the initial stage of its propagation along the oscillation chain (i.e. before the BA) obeys the power law:

$$A_{\max}(n) \sim (n_{\text{arrest}} - n)^m \tag{5}$$

It is natural to "suspect" that the true value for the exponent in Eq. (5) is $m = 2$. To corroborate this assumption, we simulate the breather propagation in longer chains and plot the "second difference" (SD) of the breather maximum amplitudes $A_{\max}$ vs. nth oscillator of the chain, which is defined as:

$$SD(n) = A_{max}(n-1) - 2A_{max}(n) + A_{max}(n+1) \tag{6}$$

For the exact value $m = 2$, the second difference value $SD(n)$ should be independent on particle index n for $2 \le n < n_{\text{arrest}} - 1$. In order to check this claim, we compute the second difference from numeric simulation data; typical results of this simulation are presented in Fig. 7.

The second difference oscillates around the constant value, before a steep decrease. These results are well in line with power law (5) for $m = 2$; the breather arrest is associated with the start of the decrease, signified by the exit of the function $SD(n)$ from the "corridor" of small oscillations.

This corridor can be easily evaluated numerically, and thus the simulation of the second difference delivers a more reliable approach for the evaluation of the BA site than just imposing the amplitude threshold. In the same time, it requires longer chains for simulation to achieve a stable asymptotic regime before BA. For the particular example of Fig. 6 we obtain $n_{\text{arrest}} = 25$; this value completely conforms to the one dictated by the imposed BA threshold $A_{\text{arrest}} = 7\times10^{-4}$.

Estimation (5) cannot hold for $n > n_{\text{arrest}}$. From the other side, the particles in the chain are physically connected even in the absence of pre-compression, and the excitation will pass along the whole chain.

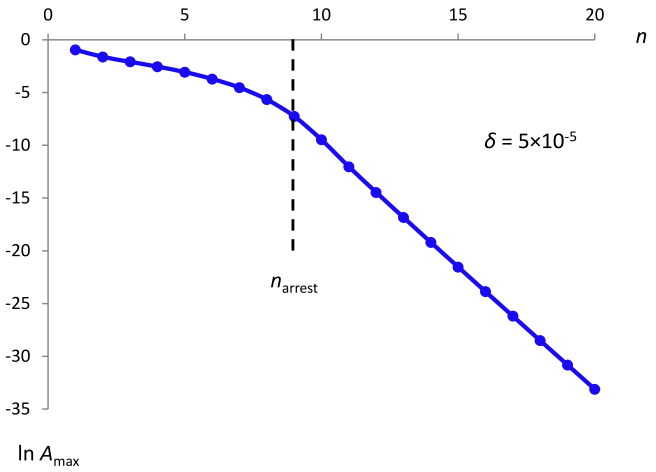

Fig. 8. Breather maximum amplitude $A_{\max}$ in the system with initial pre-compression $\delta = 5\times10^{-5}$ in semi-logarithmic scale, $A = 0.5$, $\lambda = 0.1$, $A_{\text{arrest}} = 5\times10^{-4}$ and $n_{\text{arrest}} = 9$.

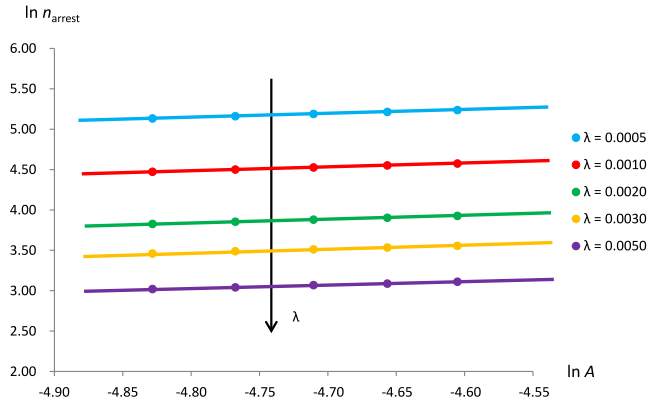

Fig. 9. n_{arrest} vs. initial velocity A in the logarithmic coordinates for different damping coefficients λ. Initial velocity range $0.008 \le A \le 0.010$.

In any realistic experimental setting, the system of granular particles presents certain non-zero pre-compression, and it should be clarified whether the BA phenomenon remains relevant in this case. System (3) thus contains the nonzero constant forces applied to the terminal particles.

In Fig. 8, we present the plot of logarithm of the maximum amplitude $A_{\max}$ of the travelling breather vs. the oscillator number n, with imposed initial pre-compression $\delta = 5\times10^{-5}$. One can observe that, if the initial pre-compression δ is small enough with respect to the initial velocity A ($\delta = A/10^4$ in the present numeric simulations), then two distinct stages of the breather propagation reveal themselves also in this case.

Thus, we can conclude that the switch of the propagation regime typical for the BA phenomenon is obtained also in the case of non-zero pre-compression. However, for the low breather amplitudes, the breather amplitude decay is exponential, as one can expect from quasi-linear system.

Now we return to the case without pre-compression, and present more detailed numeric simulations of the BA phenomenon in the space of parameters. In Fig. 9, we present the dependency of the BA depth n_{arrest} on the initial velocity within the range $0.008 \le A \le 0.010$ for a set of values of damping coefficient λ. One notes that the dependencies are reliably fitted by the straight lines, with the angular coefficients varying within the range $0.407 \le k \le 0.466$.

In Fig. 10, we present the dependence of the BA depth n_{arrest} on the damping coefficient in the range $0.0005 \le \lambda \le 0.0040$ for different values of initial velocity A. Again, linear fits work nicely, with the angular coefficients in the range $-0.931 \le l \le -0.886$.

It is then natural to assume that n_{arrest} scales with A and λ according to the approximate formula:

$$n_{\text{arrest}} \sim A^k \cdot \lambda^l \tag{7}$$

To conclude this Section, most important numeric findings are power law (5) for decay of the breather amplitude for $n < n_{\text{arrest}}$ and power law (7) for the dependence of the penetration depth on the initial amplitude of excitation and on

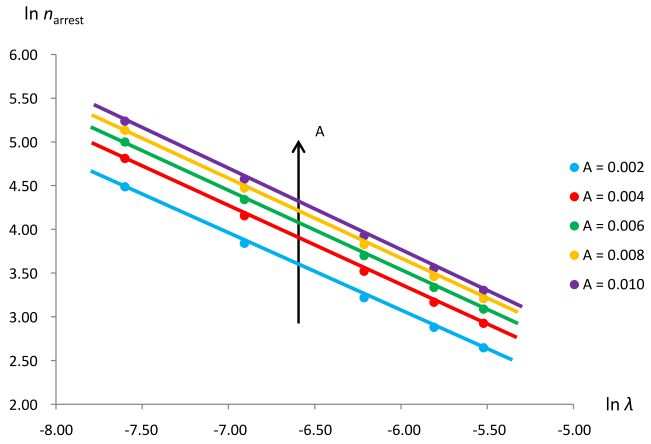

Fig. 10. n_{arrest} vs. damping coefficient λ in logarithmic coordinates for different initial velocities A. Damping coefficient range $0.0005 \leq \lambda \leq 0.0040$.

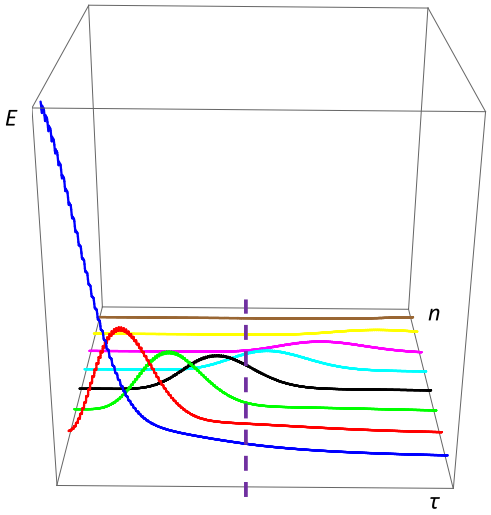

Fig. 11. Instantaneous energy $E_n(\tau)$ for $A = 0.001$, $\lambda = 0.003$. Arbitrary units for energy and time, with $1 \leq n \leq 8$.

the damping coefficient. To rationalize these findings, we analyse the simplified model of the breather propagation in the next Section.

3. Simplified model of the breather propagation

In this Section, we suggest a simplified model that mimics the breather propagation in the chain with strongly nonlinear coupling. The simplification is based on strong localization of the breather in the chain. The localization is common for excitations in granular systems. It is well-known that the solitary wave in a granular chain without the damping, on-site stiffness and pre-compression is localized on 4–5 particles [3,41]. Propagation of pulses in granular chains and lattices with on-site potentials was successfully studied in [42–44] with the help of discrete maps involving only three nearest neighbours. One can observe similar localization in the system we consider. To illustrate this fact, time series for instantaneous energies of the neighbouring particles are presented in Fig. 11. The instantaneous energy $E_n(\tau)$ of the nth oscillator is defined as a sum of oscillator kinetic energy, energy stores in the on-site spring, and half or the sum of energies of interaction with the neighbours.

One can observe that when the energy is transferred from particle n to particle $n + 1$, the particle $n + 2$ is almost not excited yet, and the particle $n - 1$ is already almost completely damped. Therefore, it is possible to assume, in a crude approximation, that the breather propagation can be understood as a sequence of energy transfers between pairs of the neighbouring particles, whereas the effect of other particles on each such transfer can be neglected. Thus, to describe the breather propagation before the arrest, one can consider a back-and forth energy transfer in a simplified model that consists only of two oscillators. These oscillators are identical to the oscillators in the initial model (Fig. 12).

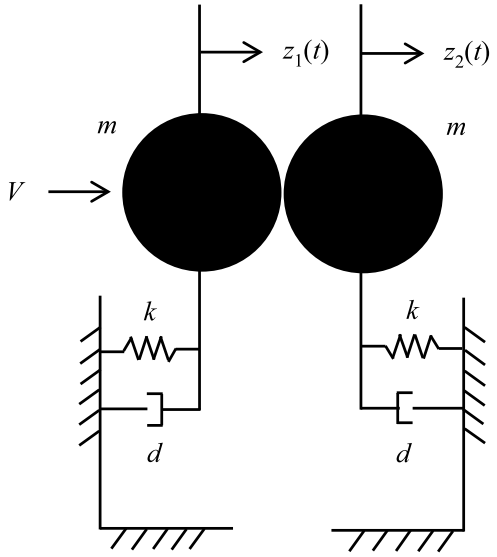

Fig. 12. Schematic configuration of the simplified 2-DOF model (no pre-compression).

One of the particles is excited with initial velocity V, and then the beatings between the oscillators occur. Each beating event is thus associated with the propagation of the breather by one particle. We are going to demonstrate that the number of such beatings will be finite, due to the strong nonlinearity of the coupling.

The case without the pre-compression is considered. The equations of motion for the 2-DOF simplified model are written as:

$$\begin{cases} \ddot{u}_1(\tau) + u_1(\tau) + \lambda \dot{u}_1(\tau) + f(u_1(\tau) - u_2(\tau)) = 0 \\ \ddot{u}_2(\tau) + u_2(\tau) + \lambda \dot{u}_2(\tau) - f(u_1(\tau) - u_2(\tau)) = 0 \end{cases} \tag{8}$$

System (8) can be uncoupled by introducing the following modal variables:

$$\begin{cases} R = \dfrac{1}{2}(u_1 + u_2) \\ w = u_1 - u_2 \end{cases} \tag{9}$$

where R is the centre of masses and w is the internal displacement of the system.

In modal coordinates, the equations of motion and initial conditions are written in the following form:

$$\begin{cases} \ddot{R} + R + \lambda \dot{R} = 0 \\ \ddot{w} + w + \lambda \dot{w} + 2f\,(w) = 0 \end{cases} \tag{10}$$

$$\begin{cases} R\,(0) = 0 \\ \mathrm{w}\,(0) = 0 \\ \dot{R}\,(0) = A/2 \\ \dot{w}\,(0) = A \end{cases} \tag{11}$$

In what follows, we assume that the damping is relatively small, in order to ensure substantial breather propagation, or number of beatings. Exact meaning of this smallness is discussed below. Then, in the basic approximation up to order $O(\lambda)$, the solution for the centre of masses R is written as:

$$R(\tau) \approx \frac{A}{2} \cdot \exp\left(-\frac{\lambda \tau}{2}\right) \cdot \sin \tau \tag{12}$$

In order to get the approximate solution for the internal displacement w of the system, we first perform the transformation to action–angle variables [45] generated by the Hamiltonian:

$$H = \frac{p^2}{2} + \frac{w^2}{2} + 2F\,(w)\,, \quad p = \dot{w}, \quad F'\,(w) = \frac{dF\,(w)}{dw} = f(w), \quad F(0) = 0 \tag{13}$$

The dependence between energy of the undamped motion and the action is determined by well-known formula [40]:

$$2\pi I = \oint p dw = 2\int_{w_{min}}^{w_{max}} \sqrt{2E(I) - w^2 - 4F(w)}dw,$$
$$\theta = \frac{\partial}{\partial I}\int_0^{w(I,\theta)} \sqrt{2E(I) - w^2 - 4F(w)}dw \tag{14}$$

where E is the energy of the undamped motion and $w_{\max,\min}$ are the maximal and minimal values of the displacement, respectively.

This canonical action–angle transformation $(p, w) \to (I, \theta)$ brings the second equation of the set (10), which is related to the internal displacement w of the system, to the following general form:

$$\dot{I} = -\lambda \cdot p(I,\theta) \cdot \frac{\partial w(I,\theta)}{\partial \theta}, \quad \dot{\theta} = \lambda \cdot p(I,\theta) \cdot \frac{\partial w(I,\theta)}{\partial I} + \frac{\partial E(I)}{\partial I} \tag{15}$$

By assuming the weak damping, one can perform the primary averaging of system (15), to obtain:

$$\dot{J} = -\frac{\lambda}{2\pi} \cdot \oint p dw = -\lambda J, \quad \langle \dot{\theta} \rangle = \frac{\partial E(J)}{\partial J}, \quad J = \langle I \rangle_\theta \tag{16}$$

Here J is the value of the action averaged with respect to the fast oscillations. The term $p(\partial w/\partial I)$ in the second equation of system (15) vanishes in the averaging, due to the invariance of the Hamiltonian (13) with respect to $p \to -p$ transformation. This invariance stems from the fact that is always possible to choose the transformations to ensure the following conditions to be fulfilled:

$$w(I,\theta) = w(I,-\theta) \Rightarrow \frac{\partial w(I,\theta)}{\partial I} = \frac{\partial w(I,-\theta)}{\partial I}, \quad p(I,\theta) = -p(I,-\theta) \tag{17}$$

Eqs. (16) are easily solvable and they yield:

$$J = J_0 \cdot \exp(-\lambda\tau), \quad \langle\theta\rangle = \theta_0 + \int_0^\tau \Omega(J_0 \cdot \exp(-\lambda\tau))d\tau, \quad \Omega = \frac{\partial E(J)}{\partial J} \tag{18}$$

Here J_0 is the initial value of the averaged action. Despite the strongly nonlinear coupling, the modal equations (10) for $w(\tau)$ contains the linear stiffness. Moreover, when discussing the breather arrest, we deal with the regime of relatively low-amplitude of beatings in system (10), where frequencies of $R(\tau)$ and $w(\tau)$ are close. It means, in turn, that also the internal displacement can be treated in the quasilinear approximation. To this end, we use the well-known action–angle transformation for linear oscillator [40]. These transformations allow one to find the relationship between the displacement and the averaged action:

$$\begin{cases} w = \sqrt{2I} \cdot \sin\theta \\ p = \dot{w} = \sqrt{2I} \cdot \cos\theta \end{cases} \to I(0) = J_0 = \frac{A^2}{2} \tag{19}$$

From expressions (18)–(19), while setting the initial phase θ_0 in (18) to 0 due to the initial conditions, one obtains the following expression for the internal displacement in the simplified 2-DOF model:

$$w \approx \sqrt{2J(\tau)} \cdot \sin\langle\theta\rangle \approx A \cdot \exp\left(-\frac{\lambda\tau}{2}\right) \cdot \sin\left(\int_0^\tau \Omega\left(\frac{A^2}{2} \cdot \exp(-\lambda\tau)\right)d\tau\right) \tag{20}$$

Estimation of the instantaneous frequency $\Omega(J)$ requires more refined analysis. In the Appendix it is demonstrated that, assuming small amplitudes in Eq. (14), one can obtain:

$$E(I) = I + \frac{2}{\pi} \cdot \int_{-1}^{1} \frac{F(\sqrt{2I} \cdot z)}{\sqrt{1-z^2}}dz + \text{H.O.T.} \tag{21}$$

Here H.O.T. stands for high-order terms. Eq. (21) is general and suitable for any nonlinear coupling, provided that the integral is not zero. If the integral in Eq. (21) turns out to be zero, these high-order terms should be analysed more thoroughly, since they provide the primary effect. However, in the case of Hertzian contact it is not the case. Namely, one adopts:

$$f(w) = \begin{cases} 0, & w \le 0 \\ w^{3/2}, & w > 0 \end{cases} \quad \Rightarrow \quad F(w) = \begin{cases} 0, & w \le 0 \\ \frac{2}{5} \cdot w^{5/2}, & w > 0 \end{cases} \tag{22}$$

Substituting (22) into (21) and performing the integration, one obtains:

$$E(I) = I + \frac{24}{25\pi} \cdot 2^{3/4} \cdot I^{5/4} \cdot \left(2\boldsymbol{E}\left(\frac{\sqrt{2}}{2}\right) - \boldsymbol{K}\left(\frac{\sqrt{2}}{2}\right)\right) \tag{23}$$

Here $\boldsymbol{K}(k)$, $\boldsymbol{E}(k)$ are complete elliptic integrals of the first and the second kind, respectively. Expression for the instantaneous frequency is obtained by simple differentiation of expression (23):

$$\begin{aligned}\Omega(\tau) &= \frac{\partial E(J)}{\partial J} = 1 + \frac{6}{5\pi}\cdot 2^{3/4}\cdot J^{1/4}\cdot\left(2\boldsymbol{E}\left(\frac{\sqrt{2}}{2}\right) - \boldsymbol{K}\left(\frac{\sqrt{2}}{2}\right)\right)\\ &= 1 + \frac{6\sqrt{2}}{5\pi}\cdot A^{1/2}\cdot\exp\left(-\frac{\lambda t}{4}\right)\cdot\left(2\boldsymbol{E}\left(\frac{\sqrt{2}}{2}\right) - \boldsymbol{K}\left(\frac{\sqrt{2}}{2}\right)\right)\end{aligned} \tag{24}$$

Substituting (24) into (20) and performing a simple integration, we obtain the following approximate expression for the time dependence of the internal displacement $w(\tau)$ as a function of the system parameters:

$$\begin{aligned}w(\tau) &\approx A\cdot\exp\left(-\frac{\lambda\tau}{2}\right)\cdot\sin\left(\tau + 2c\cdot\frac{A^{1/2}}{\lambda}\cdot\left(1-\exp\left(-\frac{\lambda\tau}{4}\right)\right)\right),\\ c &= \frac{12\sqrt{2}}{5\pi}\cdot\left(2\boldsymbol{E}\left(\frac{\sqrt{2}}{2}\right) - \boldsymbol{K}\left(\frac{\sqrt{2}}{2}\right)\right)\end{aligned} \tag{25}$$

Finally, recalling expression (9), one obtains explicit expressions for the initial variables of the problem (u_1, u_2) (derivation details are presented in the Appendix):

$$\begin{aligned}&u_1(\tau) = R(\tau) + \frac{w(\tau)}{2}\\ &\approx A\cdot\exp\left(-\frac{\lambda\tau}{2}\right)\cdot\sin\left(\tau + c\frac{A^{1/2}}{\lambda}\left(1-\exp\left(-\frac{\lambda\tau}{4}\right)\right)\right)\cdot\cos\left(c\frac{A^{1/2}}{\lambda}\left(1-\exp\left(-\frac{\lambda\tau}{4}\right)\right)\right),\\ &u_2(\tau) = R(\tau) - \frac{w(\tau)}{2}\\ &\approx A\cdot\exp\left(-\frac{\lambda\tau}{2}\right)\cdot\cos\left(\tau + c\frac{A^{1/2}}{\lambda}\left(1-\exp\left(-\frac{\lambda\tau}{4}\right)\right)\right)\cdot\sin\left(c\frac{A^{1/2}}{\lambda}\left(1-\exp\left(-\frac{\lambda\tau}{4}\right)\right)\right)\end{aligned} \tag{26}$$

Derivation of Eqs. (26) requires substantial amount of approximations. To check the validity of these approximations, we compare the approximate solutions (26) with direct numeric simulations of System (8). Typical results are presented in Fig. 13.

These results point on satisfactory accuracy of analytic approximation (26). One can notice certain discrepancy between the shapes of the modulation envelopes. Still, the number of beating cycles is predicted accurately.

At this stage, it is possible to discuss the optimal initial conditions for the breather initiation. From Eqs. (24)–(25), it follows that the characteristic frequency of the beatings may be estimated as:

$$\Omega_B \approx \frac{1}{2}\cdot\left(\frac{\partial E}{\partial I} - 1\right) = \frac{cA^{1/2}}{4} \approx 0.23\sqrt{A} \tag{27}$$

In order to obtain well-developed beatings, i.e., well-structured breather, the beating frequency Ω_B should be substantially lower than the natural frequency ω_n of the on-site potential, i.e., than unity. Therefore from (27) one can conclude that the breathers are expected only for moderate values of the excitation amplitude, i.e., for $|A| \leq 1$. This conclusion conforms to the numeric simulation data.

The breather formation also requires a substantial number of beating cycles. This number of beatings $n_{\max}$ is obtained from the last terms in Eqs. (26) that define the number of oscillatory cycles of the modulation. Then, the value of the penetration depth at the BA n_{arrest} is estimated as follows:

$$n_{\max} = n_{\text{arrest}} \approx \frac{2c}{\pi}\cdot\frac{A^{1/2}}{\lambda} \tag{28}$$

from which it emerges that the damping coefficient λ should be small enough to allow a substantial depth of the breather penetration.

Eq. (28) explains the power law numerically stated above in Eq. (7). Theoretical values of the scaling exponents $k = 1/2$ and $l = -1$ are in good agreement with the numeric findings $k = 0.466$ and $l = -0.931$ reported in the previous Section (see Figs. 8–9).

To explain the power law (5), we observe that the maxima of the beating cycles are approximately achieved at time instances when the last terms in (26) achieve zero or extrema values.

Then, the maximum amplitude $A_{\max}$ at the site n is achieved at the time instance τ_n, given by:

$$n_{\text{arrest}}\cdot\left(1-\exp\left(-\frac{\lambda\tau_n}{4}\right)\right) \approx n \tag{29}$$

By considering the expressions (26) and (29), one obtains the following estimation for the breather maximum amplitude $A_{\max}$ as the function of the chain site:

$$A_{\max}(n) \approx A\cdot\exp\left(-\frac{\lambda\tau_n}{2}\right) \approx A\cdot\left(1-\frac{n}{n_{\text{arrest}}}\right)^2 \tag{30}$$

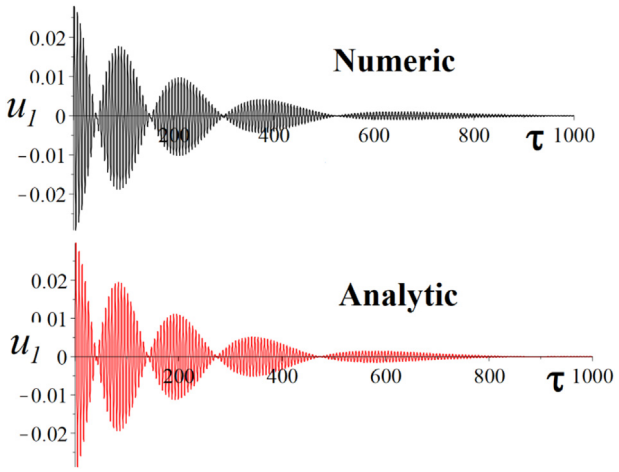

Fig. 13. Comparison between direct numeric simulations of time series for $u_1(\tau)$ from Eq. (8) (upper panel) and analytic approximation (27) (lower panel), $A = 0.03$, $\lambda = 0.01$.

Again, this last expression fits to the numeric findings of the previous Section, see Fig. 5 and Eq. (5); in particular, the theoretical scaling exponent $m = 2$ is in good agreement with the numeric value $m = 2.08$. As one can expect, Eq. (30) is valid only for finite number of sites and it does not explain the hyper-exponential propagation process represented in Fig. 4: this process is obviously beyond the validity of the simplified model pursued in this Section.

Finally, let us consider more general power law in Eq. (22):

$$f(w) = \begin{cases} 0, & w \le 0 \\ w^d, & w > 0, \end{cases} \quad d > 1 \tag{31}$$

Then, by similar evaluation, one obtains the following scaling laws:

$$n_{\text{arrest}} \approx \frac{A^{d-1}}{\lambda}, \quad A_{\max}(n) \approx A \cdot \left(1 - \frac{n}{n_{\text{arrest}}}\right)^{\frac{1}{d-1}} \tag{32}$$

Earlier paper [31] has addressed the case $d = 3$ (the potential of interaction was symmetric, but this peculiarity has no effect on scaling estimations like (32)). Numeric exploration indeed confirmed the dependence $n_{\text{arrest}} \sim A^2$ for the BA penetration depth, but the breather amplitude decay $A_{\max}(n)$ has not been explored.

To supply an additional illustration for the scaling laws (32), we present in Fig. 13 the dependence of the breather maximum amplitude $A_{\max}$ on the oscillator site n for the case $d = 3$ (i.e., cubic coupling between the neighbouring oscillators). Other parameters (initial velocity A and viscous damping λ) are listed in the caption of Fig. 14.

Data from Fig. 14 are re-plotted in semi-logarithmic scale ($\ln A_{\max}$ vs. n) in Fig. 15 and in double-logarithmic scale for modified coordinates ($\ln A_{\max}(n)$ vs. $\ln (n_{\text{arrest}} - n)$ for $n < n_{\text{arrest}}$) in Fig. 16.

In Fig. 15, one even more clearly observes the two different stages of the breather propagation pattern — power-law decay before arrest (BA penetration depth $n_{\text{arrest}} = 13$ at the BA threshold $A_{\text{arrest}} = 4\times10^{-5}$) and hyper-exponential decay after arrest, which justifies the notion of *breather arrest* also in the case of cubic coupling between the nearest oscillators.

As for the fragment $n < n_{\text{arrest}}$, according to Fig. 15, one can adopt a linear fitting between $\ln A_{\max}(n)$ and $\ln (n_{\text{arrest}} - n)$, with the approximate slope $m = 0.525$, which corroborates the estimation $A_{\max}(n) \sim (n_{\max} - n)^{1/2}$ for the pre-arrest propagation that follows from prediction (32) for $d = 3$.

4. Conclusions

We demonstrated that the combination of strongly nonlinear (non-linearizable) coupling and damping leads to qualitatively new patterns of the breather propagation in the lattice — namely, the crossover between two asymptotic regimes. The first stage, or pattern, is characterized by a relatively slow (power-law) decay of the travelling breather amplitude. The simplified model of two oscillators allows an insight into this stage and yields reasonable predictions of the power-law decay and the scaling of the penetration depth with the initial excitation amplitude and damping. Explicit formulae like (28) also yield a correct order of magnitude for the penetration depth, although a numeric coincidence is less impressive. Perhaps, it is already too much to expect from this over-simplified model.

The second stage of the breather propagation is characterized by extremely small amplitudes that decay hyper-exponentially with the penetration depth. Such additional penetration is inevitable due to the coupling inside the chain,

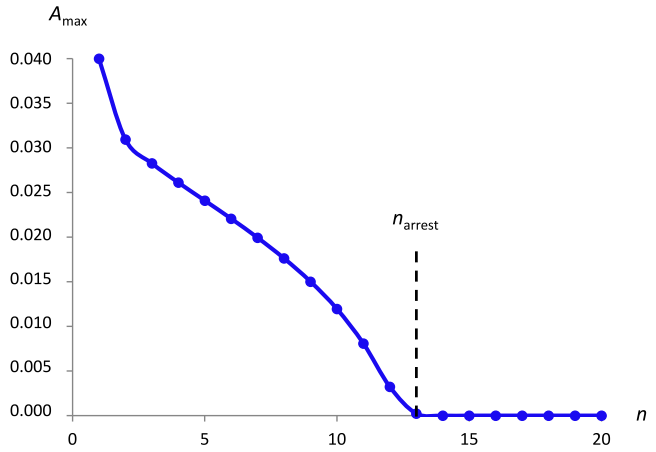

Fig. 14. Breather maximum amplitude A_{max} vs. n for cubic coupling between the nearest oscillators, $A = 0.04$, $\lambda = 5\times10^{-5}$. BA threshold $A_{arrest} = 4\times10^{-5}$. BA depth $n_{arrest} = 13$.

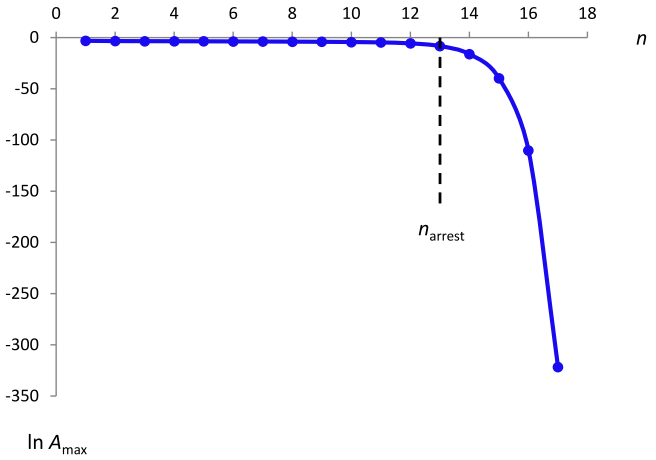

Fig. 15. Breather maximum amplitude A_{max} vs. n in semi-logarithmic coordinates for the cubic coupling, $A = 0.04$, $\lambda = 5\times10^{-5}$. BA threshold $A_{arrest} = 4\times10^{-5}$. BA depth $n_{arrest} = 13$.

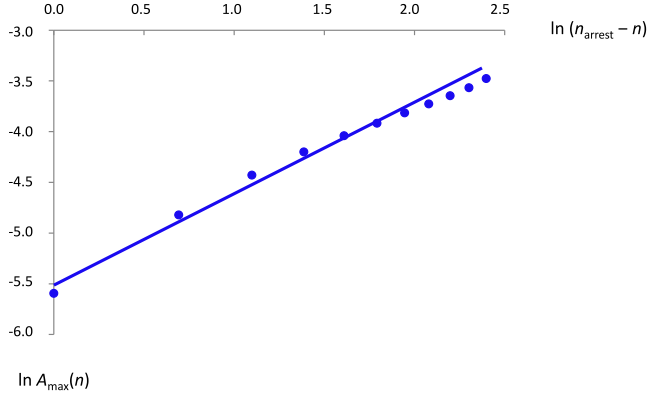

Fig. 16. Breather maximum amplitude $A_{max}(n)$ vs. $(n_{arrest} - n)$ in logarithmic coordinates for the cubic coupling, $A = 0.04$, $\lambda = 5\times10^{-5}$. BA threshold $A_{arrest} = 4\times10^{-5}$. BA depth $n_{arrest} = 13$.

but, needless to say, cannot be explained with the simplified 2-DOF model. In any case, the amplitudes in this regime are by many orders of magnitude smaller than the initial excitation, and therefore this propagation stage hardly can be

observed in any imaginable experiment. The results allow one to conjecture that the BA phenomenon reveals itself due to peculiar interaction of two generic factors — the damping and the essential coupling nonlinearity. Thus, one can expect to encounter similar pattern of the breather propagation in much broader class of possible models. One can also hope that the 2-DOF basic model will help to understand main scaling relationships at the first penetration stage. At the same time, analytic approximation (20) can become insufficient, for instance, for symmetric coupling force $f(w) = f(-w)$. In this case, more refined analysis will be required. Besides, the numeric simulations demonstrate that the crossover between two patterns of the breather propagation reveals itself also in the presence of small pre-compression.

Substantially high excitation amplitudes ($A \gg 1$) result in formation of the propagating pulse, rather than the breather. The considered model is very close to famous Newton cradle, so this result is not surprising. One can expect that the breather may be formed after substantial damping of the initial pulse energy in the course of propagation. This transition requires further exploration.

CRediT authorship contribution statement

Matteo Strozzi: Investigation, Methodology, Software, Validation, Visualization, Writing - original draft, Writing - review & editing. **Oleg V. Gendelman:** Conceptualization, Formal analysis, Funding acquisition, Investigation, Methodology, Project administration, Supervision, Writing - review & editing.

Declaration of competing interest

The authors declare that they have no known competing financial interests or personal relationships that could have appeared to influence the work reported in this paper.

Acknowledgement

The authors are grateful to Israel Science Foundation (Grant 1696/17) for financial support of this work.

Appendix

In this Appendix, we present somewhat awkward derivations of formulae from the paper body.

A.1. Derivation of estimation (21)

We start from Eq. (14), with bookkeeping small parameter ε included to express the smallness of the term $F(w)$. Precise physical conditions for this assumption will be discussed below:

$$2\pi I = 2\int_{w_{\min}}^{w_{\max}} \sqrt{2E - w^2 - 4\varepsilon F(w)}dw \underset{w=\sqrt{2E}z}{=} 4E\int_{w_{\min}/\sqrt{2E}}^{w_{\max}/\sqrt{2E}} \sqrt{1 - z^2 - \frac{2\varepsilon F(\sqrt{2E}z)}{E}}dz \tag{A.1}$$

The values of the maximal and minimal displacements in Eq. (A.1) are given from the following iterative procedure:

$$2E - w_{\max,\min}^2 - 4\varepsilon F\left(w_{\max,\min}\right) = 0 \rightarrow w_{\max,\min} = \pm\sqrt{2E} \mp \frac{2\varepsilon F\left(\sqrt{2E}\right)}{\sqrt{2E}} + O(\varepsilon^2) \tag{A.2}$$

Then, by substituting Eq. (A.2) into Eq. (A.1), one obtains:

$$2\pi I = 4E\int_{-1+\frac{\varepsilon F(\sqrt{2E})}{E}}^{1-\frac{\varepsilon F(\sqrt{2E})}{E}} \left[\sqrt{1-z^2} - \frac{\varepsilon F\left(\sqrt{2E}z\right)}{E\sqrt{1-z^2}} + O(\varepsilon^2)\right]dz \tag{A.3}$$

and therefore:

$$2\pi I = 4E\int_{-1}^{1}\sqrt{1-z^2}dz - 4\varepsilon\int_{-1}^{1}\frac{F\left(\sqrt{2E}z\right)}{\sqrt{1-z^2}}dz + O(\varepsilon^{3/2}) \tag{A.4}$$

The order $O(\varepsilon^{3/2})$ stems from the shift of the integration limits in the main term of Eq. (A.3).

Finally, once more adopting the iteration procedure, one obtains:

$$2\pi I \approx 4E\int_{-1}^{1}\sqrt{1-z^2}dz - 4\varepsilon\int_{-1}^{1}\frac{F\left(\sqrt{2E}z\right)}{\sqrt{1-z^2}}dz = 2\pi E - 4\varepsilon\int_{-1}^{1}\frac{F\left(\sqrt{2E}z\right)}{\sqrt{1-z^2}}dz \tag{A.5}$$

from which it is derived:

$$E \approx I + \frac{2\varepsilon}{\pi}\int_{-1}^{1}\frac{F\left(\sqrt{2E}z\right)}{\sqrt{1-z^2}}dz \tag{A.6}$$

Then, setting the bookkeeping small parameter ε to unity, one obtains Eq. (21).

From Eq. (A.3), it is clear that the expansion, the iterative process and the bookkeeping small parameter can be used if the following condition holds:

$$\left|\frac{F\left(\sqrt{2E}\right)}{E}\right| \ll 1 \tag{A.7}$$

In the case of Hertzian contact, by following Eq. (21) one obtains:

$$\left|\frac{F\left(\sqrt{2E}\right)}{E}\right| \sim \frac{\left(\sqrt{2E}\right)^{5/2}}{E} \sim E^{1/4} \tag{A.8}$$

Estimation (A.8) demonstrates that the above derivations are justified in the limit of low energies of the external excitation.

A.2. Derivation of expression (26)

To this end, we apply Eqs. (12), (25) and use the well-known trigonometric identity:

$$\begin{aligned} u_1(\tau) &= R(\tau) + \frac{w(\tau)}{2} = \frac{A}{2}\exp\left(-\frac{\lambda\tau}{2}\right)\left(\sin\tau + \sin\left(\tau + \frac{2cA^{1/2}}{\lambda}\left(1-\exp\left(-\frac{\lambda\tau}{4}\right)\right)\right)\right) \\ &= A\exp\left(-\frac{\lambda\tau}{2}\right)\sin\left(\tau + \frac{cA^{1/2}}{\lambda}\left(1-\exp\left(-\frac{\lambda\tau}{4}\right)\right)\right)\cos\left(\frac{cA^{1/2}}{\lambda}\left(1-\exp\left(-\frac{\lambda\tau}{4}\right)\right)\right) \end{aligned} \tag{A.9}$$

Expression for $u_2(\tau)$ is obtained in a similar way.

References

[1] C. Daraio, V.F. Nesterenko, E.B. Herbold, S. Jin, Energy trapping and shock disintegration in a composite granular medium, Phys. Rev. Lett. 96 (2006) 058002.
[2] J. Hong, Universal power-law decay of impulse energy in granular protectors, Phys. Rev. Lett. 94 (2005) 108001.
[3] S. Sen, J. Hong, J. Bang, E. Avalos, R. Doney, Solitary waves in the granular chain, Phys. Rep. 462 (2008) 21–66.
[4] F. Fraternali, M. Porter, C. Daraio, Optimal design of composite granular protectors, Mech. Adv. Mater. Struct. 17 (2010) 1–19.
[5] D. Khatri, C. Daraio, P. Rizzo, Coupling of highly nonlinear waves with linear elastic media, Proc. SPIE 7292 (2009).
[6] P. Rizzo, X. Ni, S. Nassiri, J.M. Vandenbossche, A solitary Wave-based Sensor to Monitor the Setting of Fresh Concrete, Sensors 14 (2014) 12568–12584.
[7] A. Spadoni, C. Daraio, Generation and control of sound bullets with a nonlinear acoustic lens, Proc. Natl. Acad. Sci. USA 107 (2010).
[8] I. Grinberg, A.F. Vakakis, O.V. Gendelman, Acoustic diode: Wave non-reciprocity in nonlinearly coupled waveguides, Wave Motion 83 (2018) 49–66.
[9] S. Flach, A. Gorbach, Discrete breathers: advances in theory and applications, Phys. Rep. 467 (2008) 1–116.
[10] N. Theodorakopoulos, Nonlinear physics (solitons, chaos, discrete breathers), in: Lecture notes at the University of Konstanz, 2006, pp. 1–174.
[11] P.G. Kevrekidis, Non-linear waves in lattices: past, present, future, IMA J. Appl. Math. 76 (2011) 389–423.
[12] S. Aubry, Discrete Breathers: Localization and transfer of energy in discrete hamiltonian nonlinear systems, Physica D 216 (2006) 1–30.
[13] O. Gendelman, L.I. Manevitch, Discrete breathers in vibroimpact chains: Analytical solutions, Phys. Rev. E 78 (2008) 026609.
[14] I. Grinberg, O.V. Gendelman, Discrete Breathers and Multi-Breathers in Finite Vibro-Impact Chain, Phys. Rev. E 94 (2016) 032204.
[15] I. Grinberg, O.V. Gendelman, Localization in coupled Finite Vibro-Impact Chains: Discrete Breathers and Multi-Breathers, Phys. Rev. E 94 (2016) 032204.
[16] S. Flach, C.R. Willis, Discrete breathers, Phys. Rep. 295 (1998) 181–264.
[17] I.B. Shiroky, O.V. Gendelman, Discrete breathers in an array of self-excited oscillators: exact solutions and stability, Chaos 26 (2016) 103112.
[18] O.V. Gendelman, Exact solutions for discrete breathers in forced-damped chain, Phys. Rev. E 87 (2013) 062911.
[19] N. Perchikov, O.V. Gendelman, Dynamics and stability of a discrete breather in a harmonically excited chain with vibro-impact on-site potential, Physica D 292–293 (2015) 8–28.
[20] S. Aubry, T. Cretegny, Mobility and reactivity of discrete breathers, Physica D 119 (1998) 34–46.
[21] S. Flach, K. Kladko, Moving discrete breathers?, Physica D 127 (1999) 61–72.
[22] Y. Sire, G. James, Traveling breathers in Klein-Gordon chains, C. R. Math. 338 (2004) 661–666.
[23] O. Bang, M. Peyrard, High order breather solutions to a discrete nonlinear Klein-Gordon model, Physica D 81 (1995) 9–22.
[24] Y. Sire, G. James, Numerical computation of travelling breathers in Klein-Gordon chains, Physica D 204 (2005) 15–40.
[25] G. Iooss, Travelling waves in the Fermi-Pasta–Ulam lattice, Nonlinearity 13 (2000) 849–866.
[26] I. Butt, J. Wattis, Discrete breathers in a two-dimensional Fermi-Pasta–Ulam lattice, J. Phys. A 39 (2006) 4955.
[27] M. Kastner, J.A. Sepulchre, Effective hamiltonian for traveling discrete breathers in the FPU chain, Discrete Contin. Dyn. Syst. B 5 (2005) 719–734.
[28] Y. Starosvetsky, K.R. Jayaprakash, A.F. Vakakis, Traveling and solitary waves in mono-disperse and dimer granular chains, Internat. J. Modern Phys. B 31 (2017) 1742001.
[29] Y. Starosvetsky, A.F. Vakakis, Traveling waves and localized modes in one-dimensional homogeneous granular chains with no precompression, Phys. Rev. E 82 (2010) 026603.

[30] K. Jayaprakash, A.F. Vakakis, Y. Starosvetsky, Strongly nonlinear traveling waves in granular dimer chains, Mech. Syst. Signal Process. 39 (2013) 91–107.
[31] A. Mojahed, O.V. Gendelman, A.F. Vakakis, Breather arrest, localization and acoustic non-reciprocity in dissipative nonlinear lattices, J. Acoust. Soc. Am. 146 (2019) 826–842.
[32] G. James, Nonlinear waves in the Newton's cradle and the discrete p-Schrödinger equation, Math. Models Methods Appl. Sci. 21 (2011) 2335–2377.
[33] V.F. Nesterenko, E.B. Herbold, Periodic waves in a Hertzian chain, Physics Procedia 3 (2010) 457–463.
[34] B. Bidégaray-Fesquet, E. Dumas, G. James, From Newton's cradle to discrete p-Schrödinger equation, SIAM J. Math. Anal. 45 (2013) 3404–3430.
[35] G. James, P.G. Kevrekidis, J. Cuevas, Breathers in oscillator chains with Hertzian interactions, Physica D 251 (2013) 39–59.
[36] Y. Zhang, D. Pozharskiy, D.M. McFarland, P.G. Kevrekidis, I.G. Kevrekidis A.F. Vakakis, Experimental study of nonlinear resonances and Anti-Resonances in a Forced, Ordered Granular Chain, Exp. Mech. 57 (2017) 505–520.
[37] A. Avagyan, D. Chiao, N. Dostart, K. Zhu, S. Cho, K. Remick, A.F. Vakakis, D.M. McFarland, W.M. Kriven, Experimental study of embedded and non-embedded ordered granular chains under impulsive excitation, Acta Mech. 227 (2016) 2511–2527.
[38] M.A. Hasan, S. Cho, K. Remick, A.F. Vakakis, D.M. McFarland, W.M. Kriven, Primary pulse transmission in coupled steel granular chains embedded in PDMS matrix: Experiment and modeling, Int. J. Solids Struct. 50 (2013) 3207–3224.
[39] S. Wolfram, The Mathematica Book, fourth ed., Cambridge University Press, Cambridge (UK), 1999.
[40] A. Mojahed, A.F. Vakakis, Certain aspects of the acoustics of a strongly nonlinear discrete lattice, Nonlinear Dynam. 99 (2020) 643–659.
[41] V.F. Nesterenko, Waves in strongly nonlinear discrete systems, Phil. Trans. R. Soc. A 376 (2018) 20170130.
[42] Y. Starosvetsky, Evolution of the primary pulse in one-dimensional granular crystals subject to on-site perturbations: Analytical study, Phys. Rev. E 85 (2012) 051306.
[43] Y. Ben-Meir, Y. Starosvetsky, Modulation of solitary waves and formation of stable attractors in granular scalar models subjected to on-site perturbation, Wave Motion 51 (2014) 685–715.
[44] A. Lisyansky, D. Meimukhin, Y. Starosvetsky, Primary wave transmission in the hexagonally packed, damped granular crystal with a spatially varying cross section, Commun. Nonlinear Sci. Numer. Simul. 27 (2015) 193–205.
[45] L.D. Landau, E.M. Lifshitz, Mechanics, third ed., Elsevier, 1976.